

# Robust $C^0$ high-order plate finite element for thin to very thick structures: mechanical and thermo-mechanical analysis

O. Polit<sup>\*,†</sup>, P. Vidal and M. D'Ottavio

*LEME - EA4416, Université Paris Ouest, 50 rue de Sèvres, 92410 Ville d'Avray, France*

## SUMMARY

This paper presents a new  $C^0$  eight-node quadrilateral finite element (FE) for geometrically linear elastic plates. This finite element aims at modeling both thin and thick plates without any pathologies of the classical plate finite elements (shear and Poisson or thickness locking, spurious modes, etc). A  $C^1$  FE was previously developed by the first author based on the kinematics proposed by Touratier. This new FE can be viewed as an evolution towards three directions: (1) use of only  $C^0$  FE approximations; (2) modeling of thick to thin structures; and (3) capability in multifield problems. The transverse normal stress is included allowing use of the three-dimensional constitutive law. The element performances are evaluated on some standard plate tests, and comparisons are given with exact three-dimensional solutions for plates under mechanical and thermal loads. Comparisons are made with other plate models using  $C^1$  and semi- $C^1$  FE approximations as well as with an eight node  $C^0$  FE based on the Reissner–Mindlin model. All results indicate that the present element is highly insensitive to mesh distortion, has very fast convergence properties and gives accurate results for displacements and stresses. Copyright

KEY WORDS: sinus model; normal stresses; thick plates;  $C^0$  finite element; numerical locking; mechanical load; thermo-mechanical load

## 1. INTRODUCTION

Research is still active on plate and shell finite element (FE) approximations to improve performances in terms of convergence rate and accuracy on displacements and stresses and to overcome numerical lacks such as transverse, Poisson and membrane locking, spurious modes, etc. These developments are mainly based on the classical first order shear deformation theory (FSDT), named Reissner–Mindlin for plates and Nagdhi for shells. In this research field, contributions on beam, plate, shell and three-dimensional (3D) shell FE are too extensive to be reviewed here, but readers can refer for instance to the bibliography listed in [1, 2]. In this huge literature, different techniques have been developed to overcome or control transverse shear locking. They can be associated with reduced integration, mixed approach or B-bar solution. In this last approach, the FE approximation matrix  $B$  of the transverse shear strain is replaced by a modified one, denoted  $B$ -bar. Exhaustivity is unreachable, but we can cite among others the following techniques: Kirchhoff-mode [3], mixed interpolation of tensorial components (MITC) [4], field compatibility [5], assumed natural strain (ANS) [6], discrete shear triangle (DST) [7] (considered as an extended discrete Kirchhoff triangle (DKT) formulation), enhanced assumed strain (EAS) [8], . . . and more recently, discrete strain gap (DSG) [9]. In this last contribution, a unified approach for shear-locking-free shell FE is proposed.

Furthermore, research is also active on the development of new theoretical models for heterogeneous structures and multifield problems. In this context, two families can be identified:

\*Correspondence to: O. Polit, LEME - EA4416, Université Paris Ouest, 50 rue de Sèvres, 92410 Ville d'Avray, France.

†E-mail: olivier.polit@u-paris10.fr

the equivalent single layer models (ESLM), where the classical Love–Kirchhoff (CLT) and Reissner–Mindlin (FSDT) models can be found for plates, and the layer-wise models (LWM). According to [10], the number of unknowns remains independent of the number of constitutive layers in the ESLM, whereas the same set of variables is used in each layer for the LWM. Another way for obtaining new models is based on the introduction of interface conditions into high-order models pertaining to the ESLM or to the LWM. This permits to reduce the number of unknowns and can be viewed as a ZIGZAG model. Excellent reviews have been made in the following articles [11–16] or in the most recent review [17]. The variational asymptotic method is also an interesting contribution to derive an efficient model for composite structures based on Reissner–Mindlin plate theory, see [18, 19].

The most common approximated plate theories, CLT and FSDT, are based on very few terms, three and five unknown functions over the thickness. This was motivated by the need of simplified theories giving simple formulas and equations, which could be solved by hand. Nowadays, computers can solve large problems with up to  $10^9$  unknowns, but numerical tools in computer software are always essentially based on these simplified theories.

Based on previous experiences of the authors on beams, plates and shells [20–23], this work proposes a new FE by referring to a high-order ESLM, which could be improved for heterogeneous structures. This high-order model is based on the sinus function, introduced by Touratier [24, 25] and for which FEs have been developed using a conforming approach [20, 21, 26, 27]. To avoid the use of  $C^1$  FE approximation, two additional unknown functions for bending are introduced with respect to the FSDT theory. The choice of  $C^0$  FE approximations simplifies the boundary condition definitions, and complex geometry with curved boundary can be approximated in a simple way. Furthermore, the transverse displacement is refined allowing the use of the 3D constitutive law. This is essential for thick structures and multifield problems, see [28] for piezoelectric coupling and [29] for thermal coupling. For this, two supplementary unknowns are introduced, which are statically condensed at element level. The treatment of the transverse shear locking is based on the field compatibility approach originally formulated for FSDT model [30], and here extended to high-order model.

This new eight-node quadrilateral FE with seven degrees of freedom (DOF) per node is fully described in the first two sections, in which the definition of the plate problem and the FE approximations are given. Numerical evaluations are subsequently presented which involve: locking phenomena (transverse shear and Poisson), sensitivity to distorted meshes and convergence properties for homogeneous plates under mechanical and thermal loads. A composite plate submitted to mechanical and thermal loads is finally addressed.

## 2. DESCRIPTION OF THE PLATE PROBLEM

### 2.1. Governing equations

Let us consider a plate occupying the domain  $\mathcal{V} = \Omega \times [-\frac{e}{2} \leq z \leq \frac{e}{2}]$  in a Cartesian coordinate system  $(x_1, x_2, x_3 = z)$ . The plate is defined by an arbitrary surface  $\Omega$  in the  $(x_1, x_2)$  plane, located at the midplane for  $z = 0$ , and by a constant thickness  $e$ .

*2.1.1. Constitutive relation.* The plate can be made of  $Nl$  perfectly bonded orthotropic layers. Using matrix notation, the 3D constitutive law of the  $k^{th}$  layer is given by:

$$\begin{bmatrix} \sigma_{11}^{(k)} \\ \sigma_{22}^{(k)} \\ \sigma_{33}^{(k)} \\ \sigma_{23}^{(k)} \\ \sigma_{13}^{(k)} \\ \sigma_{12}^{(k)} \end{bmatrix} = \begin{bmatrix} C_{11}^{(k)} & C_{12}^{(k)} & C_{13}^{(k)} & 0 & 0 & C_{16}^{(k)} \\ & C_{22}^{(k)} & C_{23}^{(k)} & 0 & 0 & C_{26}^{(k)} \\ & & C_{33}^{(k)} & 0 & 0 & C_{36}^{(k)} \\ & & & C_{44}^{(k)} & C_{45}^{(k)} & 0 \\ & \text{sym} & & & C_{55}^{(k)} & 0 \\ & & & & & C_{66}^{(k)} \end{bmatrix} \begin{bmatrix} \varepsilon_{11}^{(k)} \\ \varepsilon_{22}^{(k)} \\ \varepsilon_{33}^{(k)} \\ \gamma_{23}^{(k)} \\ \gamma_{13}^{(k)} \\ \gamma_{12}^{(k)} \end{bmatrix} \quad \text{that is } \left[ \sigma^{(k)} \right] = \left[ C^{(k)} \right] \left[ \varepsilon^{(k)} \right] \quad (1)$$

where we denote the stress vector  $[\sigma]$ , the strain vector  $[\varepsilon]$  and  $C_{ij}$  the 3D stiffness coefficients.

For the thermo-mechanical analysis, the 3D constitutive law is modified, introducing the thermal expansion coefficients  $\alpha_i^{(k)}$  and the variation of the temperature  $\Delta T$ , as follows:

$$\begin{bmatrix} \sigma_{11}^{(k)} \\ \sigma_{22}^{(k)} \\ \sigma_{33}^{(k)} \end{bmatrix} = \begin{bmatrix} C_{11}^{(k)} & C_{12}^{(k)} & C_{13}^{(k)} \\ & C_{22}^{(k)} & C_{23}^{(k)} \\ \text{sym} & & C_{33}^{(k)} \end{bmatrix} \begin{bmatrix} \varepsilon_{11}^{(k)} - \alpha_1^{(k)} \Delta T \\ \varepsilon_{22}^{(k)} - \alpha_2^{(k)} \Delta T \\ \varepsilon_{33}^{(k)} - \alpha_3^{(k)} \Delta T \end{bmatrix} \quad (2)$$

2.1.2. *The weak form of the boundary value problem.* Using this matrix notation and for admissible virtual displacement  $\vec{u}^* \in U^*$ , the variational principle is given by:

find  $\vec{u} \in U$  (space of admissible displacements) such that:

$$-\int_{\mathcal{V}} [\varepsilon(\vec{u}^*)]^T [\sigma(\vec{u})] d\mathcal{V} + \int_{\mathcal{V}} [u^{*T}] [f] d\mathcal{V} + \int_{\partial\mathcal{V}_F} [u^*]^T [F] d\partial\mathcal{V} = \int_{\mathcal{V}} \rho [u^*]^T [\ddot{u}] d\mathcal{V} \quad (3)$$

$\forall \vec{u}^* \in U^*$

where  $[f]$  and  $[F]$  are the prescribed body forces and surface loads applied on  $\partial\mathcal{V}_F$ , respectively.  $\varepsilon(\vec{u}^*)$  is the compatible virtual strain, and  $\rho$  is the mass density.

## 2.2. The displacement field

It is possible that it will be required that all formulations of the two-dimensional (2D) theory (still to be established) be deductions from the 3D formulation of a relevant boundary value problem. For instance, an asymptotic expansion of the displacement field can be used. But it is also possible, and often very much more practical, to establish a major part of a 2D plate theory without reference to any 3D formulation. In this last case, an approximate theory can be constructed with 2D ‘ad-hoc’ assumptions, which should lead to the same or nearly the same results as the deductive steps from three to two dimensions.

Based on the sinus model, see [24], a new plate model which takes into account the transverse normal stress is presented in this section. This extension is based on following developments

- various models for beams, plates and shells based on the refined sinus theory, [20–26, 31];
- the contributions on plates/shells of different authors on six, seven, nine parameter models, assuming a non-vanishing  $\sigma_{33}$ : see pioneer works on shell FE in [8, 32, 33] and contributions of Tessler *et al.* on the  $\{1, 2\}$  and  $\{3, 2\}$ -plate theories [34, 35].

The kinematics of our model is assumed to have the following particular form

$$\begin{cases} U_1(x_1, x_2, x_3 = z) = u_0(x_1, x_2) - z u_1(x_1, x_2) + f(z) (u_1(x_1, x_2) + \theta_2(x_1, x_2)) \\ U_2(x_1, x_2, x_3 = z) = v_0(x_1, x_2) - z v_1(x_1, x_2) + f(z) (v_1(x_1, x_2) - \theta_1(x_1, x_2)) \\ U_3(x_1, x_2, x_3 = z) = w_0(x_1, x_2) + z w_1(x_1, x_2) + z^2 w_2(x_1, x_2) \end{cases} \quad (4)$$

where  $(u_0, v_0, w_0)$  are the displacements of a point of the reference surface while  $(v_1, \theta_1)$  and  $(u_1, \theta_2)$  are measures for rotations of the normal transverse fiber about the axis  $(0, x_1)$  and  $(0, x_2)$ , respectively. Finally, the functions  $(w_1, w_2)$  permit to have a nonconstant deflection for the transverse fiber and allow to have nonzero transverse normal stress. Furthermore, the quadratic assumption for the transverse displacement avoids the occurrence of Poisson (or thickness) locking, see [36].

In the kinematics expressed by Equation (4), the two transverse shear strain components can be identified:

$$\gamma^1_{13} = u_1 + \theta_2 \quad \gamma^1_{23} = v_1 - \theta_1 \quad (5)$$

Finally, in the context of the sinus model, we have

$$f(z) = \frac{e}{\pi} \sin \frac{\pi z}{e} \quad (6)$$

It must be noticed that the classical homogeneous sinus model [24] can be recovered from Equation (4) assuming  $w_{0,1} = u_1$ ,  $w_{0,2} = v_1$  and neglecting the unknown functions  $w_1$  and  $w_2$ .

The choice of the sinus function can be justified from the 3D point of view, using the work [37]. As it can be seen in [27], a sinus term appears in the solution of the shear equation (see Equation (7) in [27]). Therefore, the kinematics proposed can be seen as an approximation of the exact 3D solution. Furthermore, the sinus function has an infinite radius of convergence, and its Taylor expansion includes not only the third order terms but all the odd terms.

### 2.3. The strain field

The compatible strain field is directly obtained from Equation (4) as

$$\begin{cases} \varepsilon_{11} = u_{0,1} - z u_{1,1} + f(z) \gamma^1_{13,1} \\ \varepsilon_{22} = v_{0,2} - z v_{1,2} + f(z) \gamma^1_{23,2} \\ \varepsilon_{33} = w_1 + 2 z w_2 \\ \gamma_{23} = w_{0,2} - v_1 + f'(z) \gamma^1_{23} + \boxed{z w_{1,2} + z^2 w_{2,2}} \\ \gamma_{13} = w_{0,1} - u_1 + f'(z) \gamma^1_{13} + \boxed{z w_{1,1} + z^2 w_{2,1}} \\ \gamma_{12} = u_{0,2} + v_{0,1} - z (u_{1,2} + v_{1,1}) + f(z) (\gamma^1_{13,2} + \gamma^1_{23,1}) \end{cases} \quad (7)$$

The contributions of  $w_1$  and  $w_2$  in the transverse shear strains, highlighted in Equation (7), will be neglected to have no derivative of  $w_1$  and  $w_2$  in the strain components. This choice allows to use only  $C^{-1}$  continuity conditions for those functions, and it turns out to be very advantageous for the finite element approximation presented in the next section. Therefore, the transverse shear strain components become:

$$\begin{cases} \gamma_{23} = \gamma^0_{23} + f'(z) \gamma^1_{23} \\ \gamma_{13} = \gamma^0_{13} + f'(z) \gamma^1_{13} \end{cases} \quad \text{with} \quad \begin{cases} \gamma^0_{23} = w_{0,2} - v_1 \\ \gamma^0_{13} = w_{0,1} - u_1 \end{cases} \quad (8)$$

and  $\gamma^1_{\alpha 3}$  is defined in Equation (5).

### 2.4. Matrix expression of the weak form of the boundary value problem

The displacement field defined in Equation (4) can be written in matrix notation using a generalized displacement vector as

$$\begin{aligned} [u]^T &= [F_u(z)][\mathcal{E}_u] \quad \text{with} \\ [\mathcal{E}_u]^T &= \left[ \begin{array}{cccccccccccc} u_0 & v_0 & w_0 & \theta_1 & \theta_2 & u_1 & v_1 & w_1 & w_2 \end{array} \right] \end{aligned} \quad (9)$$

where  $[F_u(z)]$  depends on the normal coordinate  $z$  only and is given in Appendix A.

From Equation (7), a similar expression can be deduced for the strain field as follows:

$$\begin{aligned} [\varepsilon]^T &= [F_\varepsilon(z)][\mathcal{E}_\varepsilon] \quad \text{with} \\ [\mathcal{E}_\varepsilon]^T &= \left[ \begin{array}{cccccccccccccccc} u_0 & u_{0,1} & u_{0,2} & v_0 & v_{0,1} & v_{0,2} & \theta_1 & \theta_{1,1} & \theta_{1,2} & \theta_2 & \theta_{2,1} & \theta_{2,2} & u_1 & u_{1,1} & u_{1,2} & v_1 & v_{1,1} & v_{1,2} & w_1 & w_2 & \gamma^0_{23} & \gamma^0_{13} \end{array} \right] \end{aligned} \quad (10)$$

where  $[F_\varepsilon(z)]$  is given in Appendix A.

Using the constitutive relation given in Equation (1) and the matrix notation for the displacement and strain fields Equations (9) and (10), the following expressions are obtained for each term of

Equation (3):

$$\begin{aligned}
\int_{\mathcal{V}} [\varepsilon(\bar{u}^*)]^T [\sigma(\bar{u})] d\mathcal{V} &= \int_{\mathcal{V}} [\mathcal{E}^*_{\varepsilon}]^T [F_{\varepsilon}(z)]^T [C] [F_{\varepsilon}(z)] [\mathcal{E}_{\varepsilon}] d\mathcal{V} \\
\int_{\mathcal{V}} [u^*]^T [f] d\mathcal{V} + \int_{\partial\mathcal{V}_F} [u^*]^T [F] d\partial\mathcal{V} &= \int_{\mathcal{V}} [\mathcal{E}^*_{u}]^T [F_u(z)]^T [f] d\mathcal{V} \\
&\quad + \int_{\partial\mathcal{V}_F} [\mathcal{E}^*_{u}]^T [F_u(z)]^T [F] d\partial\mathcal{V} \\
\int_{\mathcal{V}} \rho [u^*]^T [\ddot{u}] d\mathcal{V} &= \int_{\mathcal{V}} \rho [\mathcal{E}^*_{u}]^T [F_u(z)]^T [F_u(z)] [\ddot{\mathcal{E}}_u] d\mathcal{V}
\end{aligned} \tag{11}$$

where  $[C]$  stands for the 3D stiffness coefficients matrix, see Equation (1). In these last expressions, the integration throughout the thickness can be carried out, taking into account the stacking sequence of the laminate. The integration with respect to the in-plane domain  $\Omega$  is left over and discussed in the next section concerning FE approximations:

$$\begin{aligned}
\int_{\mathcal{V}} [\varepsilon(\bar{u}^*)]^T [\sigma(\bar{u})] d\mathcal{V} &= \int_{\Omega} [\mathcal{E}^*_{\varepsilon}]^T [k_{\varepsilon\varepsilon}] [\mathcal{E}_{\varepsilon}] d\Omega \quad \text{with } [k_{\varepsilon\varepsilon}] = \int_{-e/2}^{e/2} [F_{\varepsilon}(z)]^T [C] [F_{\varepsilon}(z)] dz \\
\int_{\mathcal{V}} [u^*]^T [f] d\mathcal{V} &= \int_{\Omega} [\mathcal{E}^*_{u}]^T [b_u] [f] d\Omega \quad \text{with } [b_u] = \int_{-e/2}^{e/2} [F_u(z)]^T dz \\
\int_{\mathcal{V}} \rho [u^*]^T [\ddot{u}] d\mathcal{V} &= \int_{\Omega} [\mathcal{E}^*_{u}]^T [m_{uu}] [\ddot{\mathcal{E}}_u] d\Omega \quad \text{with } [m_{uu}] = \int_{-e/2}^{e/2} \rho [F_u(z)]^T [F_u(z)] dz
\end{aligned} \tag{12}$$

The matrices  $[k_{\varepsilon\varepsilon}]$  and  $[m_{uu}]$  can be viewed as the integration over the thickness of the constitutive relations and the mass density of the plate.

We shall limit the scope of the article to static problems, for which the inertial term is neglected, see third equation of Equations (11) and (12).

Equation (12) is a good starting point for FE approximations. The generalized displacement and strain vectors defined by  $[\mathcal{E}_u]$  and  $[\mathcal{E}_{\varepsilon}]$ , see respectively Equations (9) and (10), must be approximated, and this will be described in the next section.

### 3. FINITE ELEMENT APPROXIMATIONS

This section is dedicated to the finite element approximations of the geometry and the generalized displacement and strain vectors defined in the previous section.

#### 3.1. Approximation for geometry

The eight-node quadrilateral finite element is presented in Figure 1. The in-plane coordinates

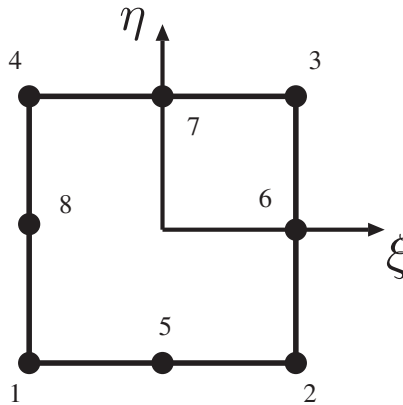


Figure 1. The reference domain of the eight-node finite element.

$(x_1, x_2)$  are approximated on the reference bi-unit domain with respect to the reduced coordinates  $(\xi, \eta)$  by

$$x_\alpha(\xi, \eta) = \sum_{i=1}^8 Nq_i(\xi, \eta)(x_\alpha)_i \quad \text{for } \alpha \in \{1, 2\} \quad (13)$$

where  $Nq_i(\xi, \eta)$  are the classical serendipity interpolation functions, see Appendix B.

### 3.2. Approximations for displacement

From Equations (9) and (10), the following functions have to be approximated:

- displacements  $(u_0, v_0, w_0)$
- rotations  $(u_1, v_1, \theta_1, \theta_2)$
- normal stretching  $(w_1, w_2)$

*3.2.1. Eight-node quadrilateral finite element.* An isoparametric procedure is used and unknown functions are approximated using the same functions as the geometry, see Equation (13). This classical approach is used for  $(u_0, v_0)$  and  $(u_1, v_1, \theta_1, \theta_2)$ .

For the transverse shear strain, and to control the transverse shear locking, a methodology was previously developed for an eight-node quadrilateral plate finite element [30, 38] based on the Reissner–Mindlin theory (FSDT) with five DOFs per node. For this, the FE approximation of the transverse displacement  $w_0$  was modified. This methodology is extended for this new FE based on a refined model and is briefly described succeedingly.

*3.2.2. Transverse shear locking.* For the constant part of the transverse shear strains, denoted  $\gamma^0$  in Equation (8), the polynomial space of the FE approximation is incompatible because each component is the sum of  $u_1$  (or  $v_1$ ) and a derivative of  $w_0$ . This is in fact the origin of the transverse shear locking, as proved in [30], implying a dependency of the convergence velocity with respect to the thickness of the plate.

A methodology named ‘field compatibility’ has been developed to avoid the transverse shear locking in the thin plate domain. This methodology is extended to the present refined model as follows:

- The constant transverse shear strains are defined in reduced coordinates:

$$\gamma_\xi^0 = u_\xi + w_{0,\xi} \quad \gamma_\eta^0 = u_\eta + w_{0,\eta} \quad (14)$$

where  $u_\xi, u_\eta$  are the projections with respect to the reduced coordinate axis of the functions  $u_1$  and  $v_1$  of Equation (4). To ensure the same polynomial approximation for the functions  $u_\xi, u_\eta$  and the derivatives of the transverse displacement in Equation (14),  $w_0$  is assumed to be cubic, introducing four supplementary DOFs at the mid-side nodes:  $(w_{0,\xi})_5, (w_{0,\eta})_6, (w_{0,\xi})_7, (w_{0,\eta})_8$ .

- A linear variation of the tangential transverse shear strain component is imposed on each side of the elementary domain, see Figure 1. Thus, the supplementary DOFs introduced at the previous step can be expressed as a linear combination of  $u_\xi, u_\eta$  and  $w_0$  DOFs. Therefore, a new finite element approximation is obtained for the transverse displacement  $w_0$ .
- The interpolation of the reduced transverse shear strain components is defined in the following polynomial basis as the intersection sets of monomial terms from  $\xi$  and  $\eta$ :

$$\begin{aligned} \mathcal{B}(\gamma_\xi^0) &= \mathcal{B}(u_\xi) \cap \mathcal{B}(w_{0,\xi}) = \{1, \xi, \eta, \xi \eta, \eta^2\} \\ \mathcal{B}(\gamma_\eta^0) &= \mathcal{B}(u_\eta) \cap \mathcal{B}(w_{0,\eta}) = \{1, \xi, \eta, \xi \eta, \xi^2\} \end{aligned} \quad (15)$$

- According to the dimension of the polynomial basis, five points are needed for each reduced transverse shear strains. These points were chosen as indicated in Figure 2 because this location

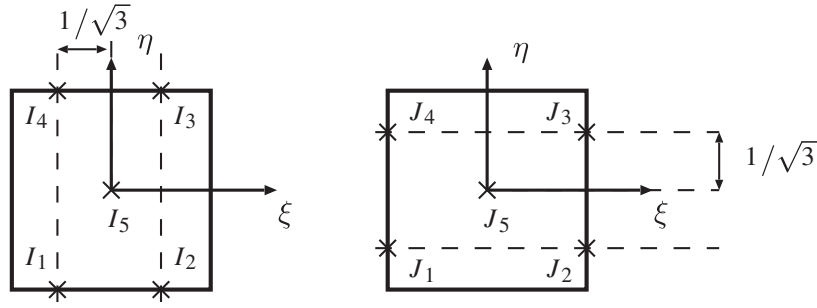


Figure 2. Point locations for the transverse shear strains evaluations.

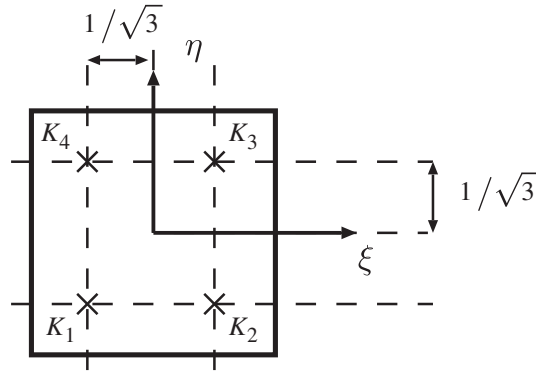


Figure 3. Internal points for the FE approximation of  $(w_1, w_2)$ .

gives the best results in case of distorted meshes, see [30, 38]. The following finite element approximation is obtained for the reduced transverse shear strains:

$$\gamma_{\xi}^0(\xi, \eta) = \sum_{I=1}^5 C_{\xi I}(\xi, \eta) \gamma_{\xi I}^0 \quad \gamma_{\eta}^0(\xi, \eta) = \sum_{J=1}^5 C_{\eta J}(\xi, \eta) \gamma_{\eta J}^0 \quad (16)$$

where  $C_{\xi I}$  and  $C_{\eta J}$  are interpolation functions, see [30].

- Using the Jacobian matrix, the physical transverse shear strains  $\gamma_{23}^0$  and  $\gamma_{13}^0$  are deduced from the reduced transverse shear strains of Equation (16).

**3.2.3. Four internal points approximation.** For the unknown functions  $(w_1, w_2)$  that are associated with the refinement of the transverse displacement, a bilinear finite element approximation is defined using four internal points denoted  $(K_i)_{i=1,4}$ , see Figure 3. The interpolation functions are given in Appendix B.

### 3.3. The elementary matrices

The elementary matrices are then deduced from Equation (12) and from the FE approximations described earlier. Because the variational principle possesses no spatial derivatives of the variables  $w_1$  and  $w_2$ , these can be condensed out statically at the element level. Therefore, the elementary stiffness matrices  $[K_e]$  can be written by referring to the retained (R) and omitted (O) DOFs:

$$[K_e] = \begin{bmatrix} K^{RR}_e & K^{RO}_e \\ K^{OR}_e & K^{OO}_e \end{bmatrix} \quad (17)$$

This matrix is associated with the following sets of DOFs:

$$\begin{aligned} [q_e^R]^T &= [ (u_0 \ v_0 \ w_0 \ \theta_1 \ \theta_2 \ u_1 \ v_1)_{i \in \{1, \dots, 8\}} ] \\ [q_e^O]^T &= [ (w_1 \ w_2)_{K_1, \dots, K_4} ] \end{aligned} \quad (18)$$

The static condensation procedure is classical and does not need to be recalled here.

For the elementary load vector, it must be noted that we are able to apply a load on the top, middle or bottom surface. Therefore, the same condensation procedure is used.

This new FE is denoted sin-z2/CL8: sinus model with a second-order expansion of the transverse displacement, and CL8 technique for the correction of the transverse shear locking. This FE has seven DOFs per node and a total of 56 DOFs on the elementary domain.

A Gaussian numerical integration using  $3 \times 3$  points is used to evaluate the elementary matrices, and a correct rank with six zero eigenvalues has been obtained. These values correspond to the six rigid body motions, so, our FE is free from spurious modes.

## 4. NUMERICAL RESULTS

In this section, several tests available in open literature are presented to evaluate the efficiency of the proposed FE. The first evaluation addresses the transverse shear and Poisson lockings. Subsequent tests consider square and circular plates to assess the sensitivity to mesh distortion. Then, isotropic square thick and thin plates are considered under mechanical and thermal loads to characterize the convergence properties for displacements and stresses. Finally, a three-layered composite plate is evaluated under mechanical and thermal loads, following the works of Pagano [39] and Bhaskar *et al.* [40].

Present results are compared with solutions obtained with previously published models [20, 21, 30], namely:

Sin/AG	Sinus model using conforming FE approximations; $C^1$ Argyris for the transverse displacement and semi- $C^1$ Ganev for in-plane displacements and rotations;
SinC/AG	Sinus model with interlayer continuity conditions using the same FE approximations;
FSDT/AG	Reissner–Mindlin model using the same FE approximations; classical shear correction factor 5/6 is used for isotropic material;
CLT/AG	Kirchhoff–Love model using the same FE approximations;
FSDT/CL8	Reissner–Mindlin model using an eight-node FE approximation and the CL8 correction for the transverse shear strain approximation; classical shear correction factor 5/6 is used for isotropic material;

Additionally, reference is made to the systematic work of Carrera and his unified formulation (CUF), see [16, 41, 42]:

ED2	Equivalent single layer model in which each displacement component is expanded to the second order; nine unknown functions are used in this kinematics;
ED3	Equivalent single layer model in which each displacement component is expanded to the third-order; twelve unknown functions are used in this kinematics.

All considered problems can make use of symmetry considerations and only a quarter-plate model is used. The meshes and the notations are presented in Figure 4.

The definition of the boundary conditions is as simple as for FSDT because same boundary conditions are applied to the DOFs  $(u_1, \theta_2)$  and  $(v_1, \theta_1)$  associated with the deformation of the transverse normal fiber. Therefore, the boundary conditions used in the evaluation are described in Table I, where 0 indicates that the DOF is fixed.

### 4.1. The locking phenomenon

**4.1.1. Transverse shear locking.** A definition of this locking is given by Babuska [43] as a non-uniformity of the convergence with respect to the thickness. Therefore, there are two ways of assessing the sensitivity to transverse shear locking:

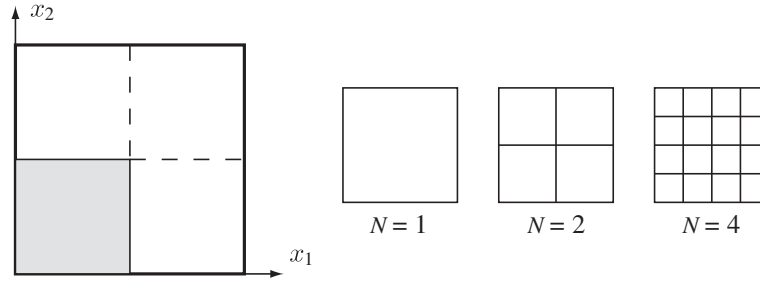


Figure 4. The meshes used for the numerical evaluations.

Table I. Definition of the boundary conditions.

DOF	$u_0$	$v_0$	$w_0$	$\theta_1$	$\theta_2$	$u_1$	$v_1$
Clamped							
$x_\alpha = cst$	0	0	0	0	0	0	0
Simply supported: SA-1							
$x_1 = cst$	0		0		0	0	
$x_2 = cst$		0	0				0
Simply supported: SA-2							
$x_\alpha = cst$			0				
Symmetry conditions							
$x_1 = cst$	0				0	0	
$x_2 = cst$		0		0			0

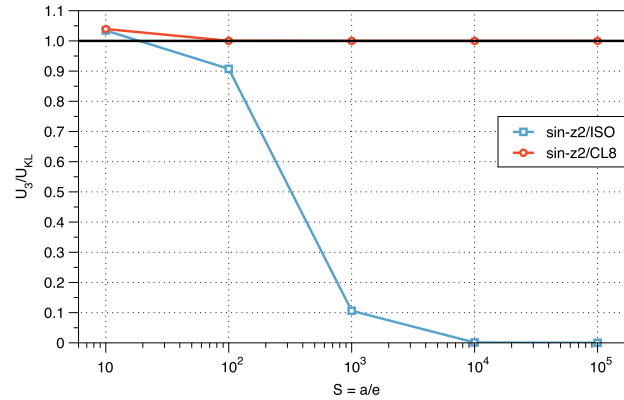


Figure 5. Transverse displacement with respect to length-to-thickness ratio.

- constant mesh, varying length-to-thickness ratio
- convergence analysis for a thick and a thin plate.

Therefore, the following test is considered:

geometry	square plate $a \times a$ and thickness $e = 10^{-n}$ with $n \in \{0, 4\}$
boundary conditions	simply supported on all sides, uniform transverse load $p_0$
materials	isotropic with $E = 10.92$ and $\nu = 0.3$
mesh	$N = 2$ (for the quarter of the plate, see Figure 4)
results	the transverse displacement at the center of the plate for $z = 0$ ,
reference value	Kirchhoff–Love theory: $U_3(a/2, a/2, 0) = 0.00406 p_0 \frac{a^4}{e^3 D}$ ; $D = E/12 (1 - \nu^2)$ .

The results are presented in Figure 5 in which the isoparametric and CL8 approximations for the constant part of the transverse shear strain  $\gamma^0$  are compared. It is obvious that the CL8 approximation is very efficient to avoid the transverse shear locking, and the mesh  $N = 2$  is sufficient to

obtain a very accurate transverse displacement, independently of the plate thickness. The isoparametric approach reveals a very strong locking. Because the reference KL solution is inadequate for semi-thick to thick plates, a discrepancy appears between the present sin-z2/CL8 and the reference results for  $S \leq 10^2$  in Figure 5.

A convergence study using meshes ( $N = 1, 2, 4, 8, 16$ ) is presented in Figure 6 for  $S = 10$  and  $S = 10^5$  with respect to the 3D elasticity solutions. A comparison is given between the isoparametric approximation and the CL8 methodology. For a thick plate ( $S = 10$ ), the CL8 methodology improves the accuracy for coarse meshes, and for a thin plate ( $S = 10^5$ ), the locking is avoided.

4.1.2. *Poisson locking.* The following test is considered:

geometry	square plate $a \times a$ and three length-to-thickness ratios $S = \frac{a}{e} = 4, 10, 100$
boundary conditions	simply supported on all sides, uniform transverse load $p_0 = 1$ .
materials	isotropic with $E = 10.92$ and three values for the Poisson ratio $\nu = 0., 0.3, 0.45$
mesh	$N = 2$
results	the transverse displacement at the center of the plate for $z = 0$ ; percent error with respect to the $N = 8$ mesh result namely $(sol - sol_{ref})/sol_{ref} \times 100$

The results are given in Table II by comparing two expansions for  $U_3$ , that is, the expansion as in Equation (4) with  $(w_i)_{i=0,1,2}$  and a linear one that neglects the second order term  $w_2$ . No locking is found for the first case, whereas without  $w_2$ , a severe locking appears. It increases with the Poisson coefficient (Poisson locking). There is no sensitivity of the results to the length-to-thickness ratio  $S$ . Therefore, if a constant or a linear variation of the transverse displacement is assumed and the 3D constitutive relation is used, the Poisson locking appears. In this case, the reduced 2D constitutive

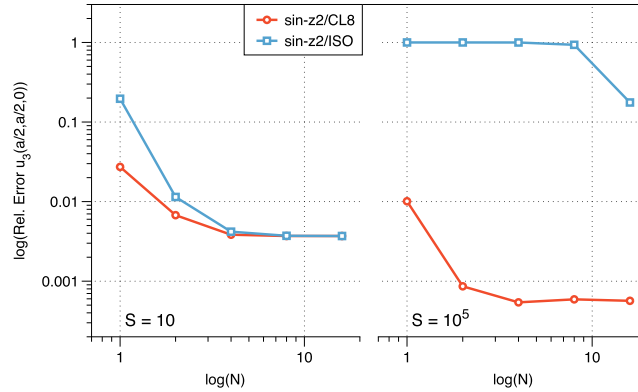


Figure 6. Convergence of the transverse displacement for two length-to-thickness ratios.

Table II. Effect of the Poisson locking.

	Percent error $U_3(a/2, b/2, 0)$	
	$(w_i)_{i=0,1,2}$	$(w_i)_{i=0,1}$
$S = 4$		
$\nu = 0$	-0.31	-0.31
$\nu = 0.3$	-0.42	-11.47
$\nu = 0.45$	-0.52	-49.84
$S = 10$		
$\nu = 0$	-0.24	-0.24
$\nu = 0.3$	-0.31	-12.28
$\nu = 0.45$	-0.39	-62.44
$S = 100$		
$\nu = 0$	-0.05	-0.05
$\nu = 0.3$	-0.06	-18.39
$\nu = 0.45$	-0.11	-66.91

law for the bending is necessary to overcome this locking, and a physical significance is proposed in [44] for shell formulation.

#### 4.2. The distortion tests

4.2.1. *Square plate test.* This test is often used to investigate the mesh sensitivity in plate bending problems [45], where a standard eight-node brick element is presented. The following data are considered, see Figure 7:

geometry	square plate of length $a = 100$ and thickness $e = 1$ ;
boundary conditions	clamp on all edges; concentrated load $F_3 = 178.5714$ at the center ;
materials	isotropic with $E = 10.92 \cdot 10^4$ and $\nu = 0.3$
mesh	$N=2$ with the parameter $s \in \{0, 4, 8, 12\}$ defining the distortion (see Figure 7),
result	displacement $U_3$ at the center for $z = 0$ ,
reference value	Kirchhoff–Love solution given by $U_3 = 0.0056 F_3 \frac{L^2}{e^3 D} = 1$ with $D = \frac{E}{12(1 - \nu^2)}.$

Two distorted meshes ( $s = 4, 12$ ) and the regular mesh ( $s = 0$ ) are presented in Figure 7 (right). For the most distorted mesh ( $s = 12$ ), the coordinates of the center node are  $(37, 37)$ , whereas the middle point coordinates of the straight line connecting the two corner nodes are  $(37.5, 37.5)$ . The transverse displacement is presented in Table III. For the regular mesh, a discrepancy of 0.1% is obtained for the maximum deflection, whereas the error is always less than 7% for all the distorted meshes. With these results and in comparison with the eight-node 3D-shell FE [45], this FE appears to be very robust with respect to distortion sensitivity.

4.2.2. *Circular isotropic plate.* This test is also presented to evaluate the sensitivity to mesh distortion and the effect of different boundary conditions. The following data are considered:

geometry	circular plate with radius $R = 5$ and two thicknesses $e = 1$ . and $0.1$ ;
boundary conditions	simply supported (SA-2) avoiding only transverse displacement, and clamped (ENC); uniform transverse load of $p_0 = 10^{-4}$
materials	isotropic with $E = 1.7472 \cdot 10^7$ and $\nu = 0.3$
mesh	$N = 1; 3; 12; 28$ for the quarter of the circular plate, see Figure 8

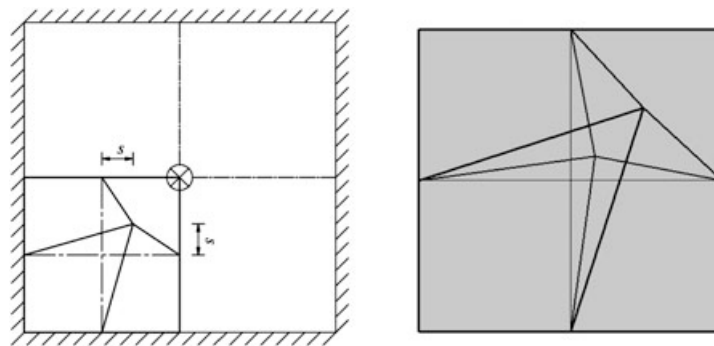


Figure 7. Clamped square plate used for mesh sensitivity (left) and meshes for  $s = 0, 4, 12$  (right).

Table III. Clamped square plate results: transverse displacement at the center

$s$	0	4	8	12
sin-z2/CL8	1.001	0.9836	0.9629	0.9366
Q1A2E11 [45]	0.868	0.8560	0.8100	—

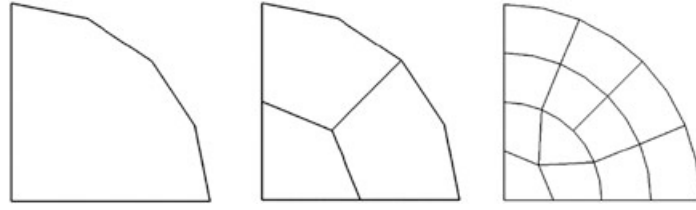


Figure 8. The finite element discretizations ( $N = 1, 3, 12$ ) of the circular plate (quarter-plate model).

Table IV. Transverse displacement for circular plate.

N	sin-z2/CL8	(%)	sin-z2/ISO	(%)	FSDT/CL8	(%)
$e = 1.;$ ENC Kirchhoff–Love ref. solution: 0.72196E-09						
1	0.61477E-09	-14.8	0.40546E-09	-43.8	0.63741E-09	-11.7
3	0.73813E-09	2.2	0.68148E-09	-5.6	0.71880E-09	-0.4
12	0.72668E-09	0.7	0.69270E-09	-4.1	0.72189E-09	0.0
28	0.72393E-09	0.3	0.71815E-09	0.3	0.72421E-09	0.3
$e = 0.1;$ ENC Kirchhoff–Love ref. solution: 0.61147E-06						
1	0.63716E-07	-89.6	0.65980E-08	-98.9	0.74789E-07	-87.8
3	0.61606E-06	0.8	0.32661E-06	-46.6	0.61528E-06	0.6
12	0.61201E-06	0.1	0.39673E-06	-35.1	0.61200E-06	0.1
28	0.61392E-06	0.4	0.55736E-06	-8.8	0.61391E-06	0.4
$e = 1.;$ SA-2 Kirchhoff–Love ref. solution: 0.25997E-08						
1	0.25659E-08	-1.3	0.20555E-08	-20.9	0.24999E-08	-3.9
3	0.25915E-08	-0.3	0.24965E-08	-4.0	0.26020E-08	-0.1
12	0.25786E-08	-0.8	0.24717E-08	-4.9	0.26044E-08	-0.2
28	0.25777E-08	-0.8	0.25620E-08	-1.5	0.26089E-08	-0.3
$e = 0.1;$ SA-2 Kirchhoff–Love ref. solution: 0.24895E-05						
1	0.22962E-05	-7.8	0.30000E-06	-87.9	0.22804E-05	-8.7
3	0.24960E-05	0.3	0.14986E-05	-39.8	0.24963E-05	0.3
12	0.24942E-05	0.2	0.16441E-05	-34.0	0.24945E-05	0.2
28	0.24891E-05	0.0	0.22819E-05	-8.3	0.24905E-05	0.0

result displacement  $U_3$  at the center,  
reference values Kirchhoff–Love solutions.

Table IV reports the results obtained with the present sin-z2 FE using isoparametric and CL8 approximations, and also with the FSDT/CL8 FE. The classical shear correction factor of  $5/6$  is used for the latter model. Sin-z2/CL8 and FSDT/CL8 behave in a similar manner. For the small thickness  $e = 0.1$ , sin-z2/ISO exhibits transverse shear locking for both boundary conditions, and convergence is very slow. Not that convergence velocity of the FE based on CL8 approximation is not sensitive to thickness. Furthermore, convergence of CL8 FE is faster with errors less than 1% using  $N = 3$  mesh. The only exception is the ( $e = 1$  ENC) case, where the error using  $N = 3$  mesh is 2.2%.

### 4.3. Homogeneous plates

4.3.1. *Mechanical analysis.* An isotropic square plate with different length-to-thickness ratios is analyzed. The following data are considered:

geometry square plate  $a \times a$  and length-to-thickness ratios  $S = \frac{a}{e} = 2, 5, 10, 100$ ;  
boundary conditions simply supported on all sides with a bi-sinusoidal transverse distributed load on the top surface  $p_3(x_1, x_2, z = \frac{e}{2}) = p_0 \sin \frac{\pi x_1}{a} \sin \frac{\pi x_2}{a}$   
materials isotropic with  $E = 73$  GPa and  $\nu = 0.34$

mesh results  $N = 1, 2, 4, 8, 16$  for the quarter of the plate  
displacements and stresses are made non-dimensional according to  

$$\bar{U}_1 = U_1(0, a/2, -e/2) \frac{E e^2}{p_0 a^3}; \bar{U}_3 = U_3(a/2, a/2, e/2) \frac{100 E e^3}{p_0 a^4}$$

$$\bar{\sigma}_{11} = \sigma_{11}(a/2, a/2, e/2) \frac{1}{p_0 S^2}; \bar{\sigma}_{13} = \sigma_{13}(0, a/2, 0) \frac{1}{p_0} S$$
reference values are the 3D exact elasticity results obtained as in [46].

A convergence study is first conducted to evaluate the convergence velocity for displacement and stresses for thin  $S = 100$  and very thick  $S = 2$  plates. Results are shown in Figure 9. Convergence velocity is high, and the error is less than 1% with the mesh  $N = 2$  for the transverse displacement  $U_3$ . For the in-plane stress  $\sigma_{11}$ , and the transverse shear stress  $\sigma_{23}$ , error is less than 3% for all length-to-thickness ratios. For the transverse normal stress, the distribution with respect to the thickness at the center of the plate is presented in Figures 11 and 12 (left) for the very thick and thin plates, respectively. The reference solution using ED4 is also given in these figures. Using the discretizations  $N = 8$  and  $N = 16$ , ratios  $sr1 = 0.65$  and  $sr2 = 0.75$  associated with the size of two adjacent finite elements are introduced, see Figure 10. For the very thick plate, see Figure 11, the distribution is not sensitive to the mesh, whereas for the thin case,  $\sigma_{33}$  is very sensitive to the mesh refinement, see the right curve of Figure 12.

Using the mesh  $N = 8$ , comparisons with other FE and the systematic approach using CUF are given in Table V for different length-to-thickness ratios. For all length-to-thickness ratios, including very thick case, the robustness of this new FE is obvious, and very good results are obtained with respect to reference elasticity solutions. Present results lie between those of ED2 and ED3 models, but are obtained with a lower number of unknown functions. With respect to FSDT model, results are largely improved on displacement and stresses, especially in the semi-thick to thick range. For semi-thick to thin plate, the results given by the present FE are of the same order of those obtained

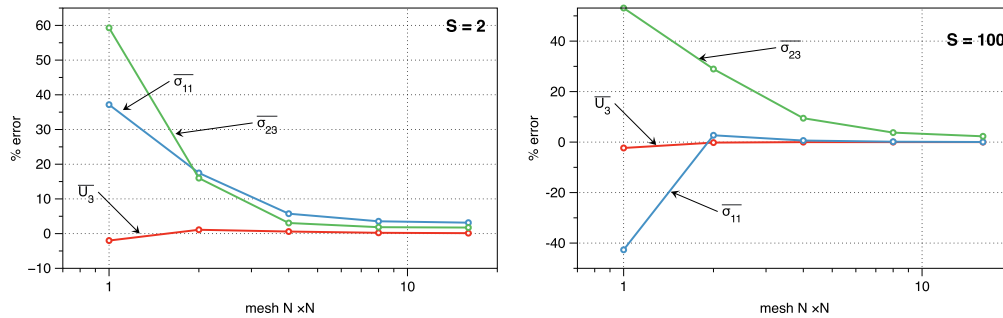


Figure 9. Isotropic square plate under mechanical load; convergence for displacement and stresses.

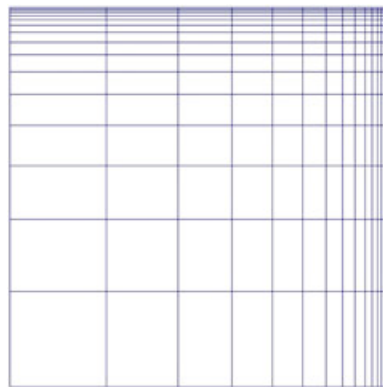


Figure 10. Non regular mesh:  $N = 16$  with  $sr2 = 0.75$ .

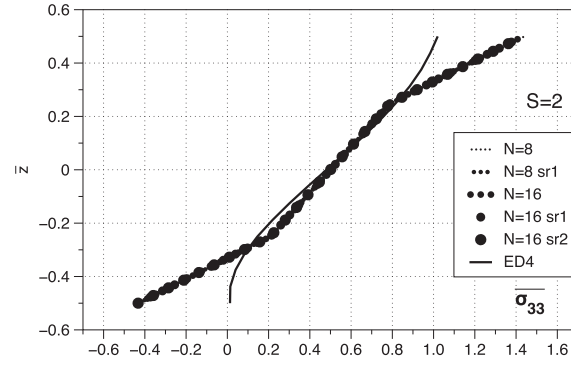


Figure 11. Isotropic square plate under mechanical load; convergence of  $\sigma_{33}/p_0$  for  $S = 2$ .

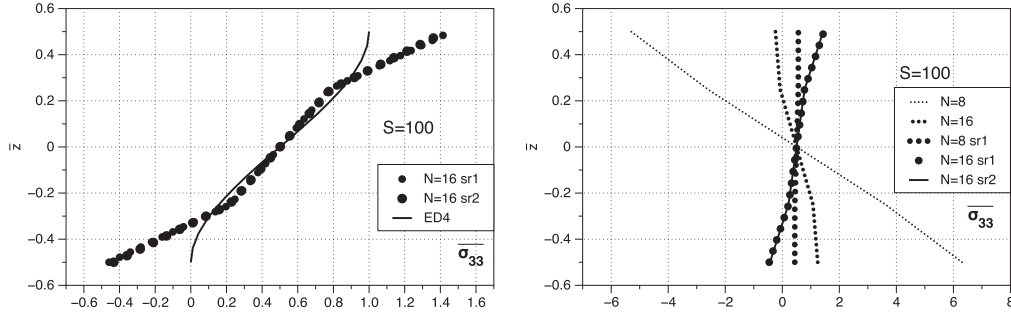


Figure 12. Isotropic square plate under mechanical load; convergence of  $\sigma_{33}/p_0$  for  $S = 100$ .

by  $\text{Sin}/\text{AG}$ . For thick plates ( $S = 2, 5$ ),  $\text{sin-z2}/\text{CL8}$  performs always better, and a good agreement with the reference solution is found.

There are 1344 DOFs for  $\text{sin-z2}/\text{CL8}$  with mesh  $N = 8$  and 760 DOFs for  $\text{Sin}/\text{AG}$  with mesh  $N = 4$ , but the bandwidth is respectively 189 and 230. Furthermore, the number of integration points are respectively 9 and 16. Therefore, this new FE seems very attractive for homogeneous plates, if we examine the ratio between computational cost and accuracy.

**4.3.2. Thermo-mechanical analysis.** This section is dedicated to the evaluation of this FE for a square plate subjected to a thermal load. The test is detailed as follows:

geometry square plate  $a \times a$  and length-to-thickness ratios  $S = \frac{a}{e} = 4, 10, 100$ ;  
 boundary conditions simply supported on all sides; the thermal load is given by

$$T(x_1, x_2, z) = T_0 \frac{2z}{e} \sin \frac{\pi x_1}{a} \sin \frac{\pi x_2}{a}$$

materials one transverse isotropic layer with  $E_L = 25 \text{ GPa}$ ,  $E_T = 1 \text{ GPa}$ ,  $\nu_{LT} = 0.25$ ,  $G_{LT} = 0.2 \text{ GPa}$ ,  $G_{TT} = 0.5 \text{ GPa}$ ; the thermal expansion coefficients are defined by  $\alpha_T = 1125 \alpha_L$

mesh  $N = 8$  for the quarter of the plate

results displacements and stresses are made non-dimensional according to

$$\bar{U}_\alpha = U_\alpha \frac{1}{T_0 \alpha_L a} \text{ for } \begin{cases} U_1(0, a/2, e/2) \\ U_2(a/2, 0, e/2) \end{cases} \quad \bar{U}_3 = U_3(a/2, a/2, e/2) \frac{e}{T_0 \alpha_L a^2}$$

$$\bar{\sigma}_{ij} = \sigma_{ij} \frac{1}{T_0 \alpha_L E_T} \text{ for } \begin{cases} \sigma_{11}, \sigma_{22}(a/2, a/2, e/2) \\ \sigma_{12}(0, 0, e/2) \\ \sigma_{13}(0, a/2, e/6) \\ \sigma_{23}(a/2, 0, e/6) \end{cases}$$

Table V. Isotropic square plate under mechanical load.

S/mesh	Model	$\bar{U}_1(\times 10^{-2})$	$\bar{U}_3$	$\bar{\sigma}_{11}$	$\bar{\sigma}_{13}$
100	Ref.	4.2788	2.7248	0.2037	0.2387
$N = 8$	Sin-z2/CL8	4.2787	2.7247	0.2038	0.2442
$N = 4$	Sin/AG	4.2790	2.7254	0.2036	0.2464
$N = 4$	FSDT/AG	4.2785	2.7254	0.2036	0.1592
	ED2	4.2785	2.7247	0.2037	0.1727
	ED3	4.2785	2.7248	0.2037	0.2387
10	Ref.	4.3057	2.8345	0.2068	0.2383
$N = 8$	Sin-z2/CL8	4.3043	2.8210	0.2090	0.2428
$N = 4$	Sin/AG	4.3238	2.8863	0.2058	0.2462
$N = 4$	FSDT/AG	4.2785	2.8867	0.2036	0.1592
	ED2	4.2762	2.8156	0.2055	0.1722
	ED3	4.3056	2.8345	0.2082	0.2383
5	Ref.	4.3765	3.2056	0.2168	0.2371
$N = 8$	Sin-z2/CL8	4.3747	3.1573	0.2244	0.2411
$N = 4$	Sin/AG	4.4594	3.3722	0.2318	0.2455
$N = 4$	FSDT/AG	4.2784	3.3755	0.2036	0.1592
	ED2	4.2565	3.1270	0.2118	0.1709
	ED3	4.3747	3.2044	0.2224	0.2372
2	Ref.	4.5017	7.3826	0.3145	0.2277
$N = 8$	Sin-z2/CL8	4.7470	7.3923	0.3244	0.2317
$N = 4$	Sin/AG	5.3883	6.7038	0.2564	0.2411
$N = 4$	FSDT/AG	4.2785	6.7968	0.2036	0.1592
	ED2	3.7200	6.7598	0.2839	0.1618
	ED3	4.4412	7.3337	0.3460	0.2287
$N = 4$	CLT/AG	4.2785	2.7238	0.2036	

Table VI. Thermal load for the homogeneous square plate.

S	Model	$\bar{U}_1$	$\bar{U}_2$	$\bar{U}_3$	$\bar{\sigma}_{11}$	$\bar{\sigma}_{22}$	$\bar{\sigma}_{12}$	$\bar{\sigma}_{13}$	$\bar{\sigma}_{23}$
4	Ref.	-16.244	-90.676	37.652	1043.40	-829.7	-167.95	104.210	-126.930
	Sin-z2/CL8	-12.517	-86.795	42.200	746.80	-845.3	-156.13	121.580	-128.340
	Sin/AG	-13.328	-85.201	21.199	811.30	-846.4	-160.68	125.380	-130.060
	FSDT/AG	-8.9449	-97.255	21.735	474.90	-811.8	-173.48	83.910	-83.960
10	Ref.	-16.017	-33.061	15.577	980.17	1011.3	-77.09	70.620	-72.960
	Sin-z2/CL8	-15.323	-32.357	16.279	926.37	-1013.7	-74.96	73.540	-74.280
	SIN/AG	-15.311	-32.092	12.764	926.03	-1012.2	-79.91	74.190	-74.700
	FSDT/AG	-14.286	-34.726	12.789	846.81	-1004.7	-83.02	48.230	-48.280
100	Ref.	-15.991	-16.177	10.240	964.81	-1064.5	-50.530	7.961	-7.964
	Sin-z2/CL8	-15.984	-16.169	10.240	966.02	-1063.9	-50.550	8.143	-8.141
	SIN/AG	-15.870	-16.223	10.140	958.11	-1062.0	-53.38	8.097	-8.104
	FSDT/AG	-15.858	-16.251	10.140	957.18	-1061.9	-53.49	5.237	-5.235
	CLT/AG	-15.876	-16.048	10.120	958.94	-1064.0	-51.69	—	—

The results are given in Table VI using the mesh  $N = 8$ . For the thin plate ( $S = 100$ ), all models give almost the same results, and CLT can be used. For semi-thick ( $S = 10$ ) and thick plates ( $S = 4$ ), the present FE gives best results. Note that in the thick case, a coefficient two is observed for the transverse displacement between present Sin-z2/CL8 and Sin/AG or FSDT/AG. The stresses obtained by Sinus models are of the same accuracy and closer to the reference solutions than the FSDT results. The use of the 3D constitutive law is, hence, proved to be mandatory to capture the effect of the thermal expansion coefficients in the three directions for the thick cases.

#### 4.4. Three-layered plates

**4.4.1. Mechanical analysis.** A composite plate is analyzed to assess this new FE plate for multilayered structures. Authors are aware that laminated structures need high-order model based for example, on a ZIGZAG theory or on a layer-wise description. The purpose of this tests is to propose a first assessment of this simple FE in the field of composite structures. The plate test is as follows:

geometry	square plate $a \times a$ and length-to-thickness ratios $S = \frac{a}{e} = 4, 10, 100$ ; three layers of equal thickness, $e/3$
boundary conditions	simply supported on all sides, a bi-sinusoidal transverse distributed load is applied on the top surface $p_3(x_1, x_2, z = \frac{e}{2}) = p_0 \sin \frac{\pi x_1}{a} \sin \frac{\pi x_2}{a}$
materials	cross-ply ( $0^\circ, 90^\circ, 0^\circ$ ) laminate and $E_L = 25$ GPa, $E_T = 1$ GPa, $\nu_{LT} = 0.25$ , $G_{LT} = 0.2$ GPa, $G_{TT} = 0.5$ GPa
mesh	$N = 16$ for the quarter of the plate; $N = 8$ is used for FE based on AG interpolations.
results	displacements and stresses are made non-dimensional according to

$$\bar{U}_\alpha = U_\alpha \frac{E_L}{p_0} e S^3 \text{ for } \begin{cases} U_1(0, a/2, -e/2) \\ U_2(a/2, 0, -e/2) \end{cases} \quad \bar{U}_3 = U_3(a/2, a/2, 0) \frac{100 E_L}{p_0 e S^4}$$

$$\bar{\sigma}_{\alpha\beta} = \sigma_{\alpha\beta} \frac{1}{p_0 S^2} \text{ for } \begin{cases} \sigma_{11}(a/2, a/2, e/2), \sigma_{22}(a/2, a/2, -e/6) \\ \sigma_{12}(0, 0, -e/2) \end{cases}$$

$$\bar{\sigma}_{\alpha 3} = \sigma_{\alpha 3} \frac{1}{p_0 S} \text{ for } \begin{cases} \sigma_{13}(0, a/2, 0) \\ \sigma_{23}(a/2, 0, 0) \end{cases}$$

reference values are the 3D exact elasticity results given in [39].

The results are presented in Table VII. Good agreement is obtained by Sin-z2/CL8 with respect to the reference values for all length-to-thickness ratios. For the thick plate, some distributions with respect to the thickness and comparisons with Sin/AG results are also given in Figure 13 for  $U_i$  and in Figures 14–16 for the stresses. The agreement between the previously developed  $C^1$  FE and the present  $C^0$  FE is obvious. The distribution over the thickness of  $U_3$  is non-constant using sin-z2/CL8, see the right curve of Figure 13. The only discrepancy is located at the top and bottom surfaces for the transverse shear stresses, see Figure 16, where the traction-free boundary conditions are not exactly recovered. This is due to the constant term of the transverse shear strain  $\gamma^0$ , see Equation (8), which is not exactly zero. Note that the free top and bottom boundary conditions are exactly satisfied using the  $C^1$  FE based on the sinus model.

Table VII. ( $0^\circ, 90^\circ, 0^\circ$ ) square plate under mechanical load.

$S$	Model	$\bar{U}_1$	$\bar{U}_2$	$\bar{U}_3$	$\bar{\sigma}_{11}$	$-\bar{\sigma}_{22}$	$\bar{\sigma}_{12}$	$\bar{\sigma}_{13}$	$\bar{\sigma}_{23}$
4	Ref.	0.0094	0.0228	2.0059	0.8008	0.5563	0.0505	0.2559	0.2172
	Sin-z2/CL8	0.0094	0.0218	2.0306	0.7617	0.5056	0.0491	0.2110	0.1864
	Sin/AG	0.0094	0.0229	1.9345	0.7554	0.5033	0.0507	0.2113	0.1877
	SinC/AG	0.0107	0.0218	1.9622	0.8560	0.5838	0.0510	0.2774	0.1494
	FSDT/AG	0.0054	0.0181	1.7758	0.4370	0.4774	0.0369	0.1201	0.1301
10	Ref.	0.0074	0.0111	0.7530	0.5906	0.2882	0.0290	0.3573	0.1228
	Sin-z2/CL8	0.0073	0.0106	0.7186	0.5857	0.2737	0.0281	0.2732	0.1046
	Sin/AG	0.0072	0.0106	0.7180	0.5727	0.2708	0.0279	0.2583	0.1059
	SinC/AG	0.0075	0.0110	0.7533	0.5975	0.2908	0.0279	0.3744	0.0859
	FSDT/AG	0.0064	0.0096	0.6693	0.5134	0.2536	0.0252	0.1363	0.0762
100	Ref.	0.0068	0.0068	0.4347	0.5393	0.1808	0.0214	0.3947	0.0828
	Sin-z2/CL8	0.0068	0.0068	0.4343	0.5396	0.1808	0.0214	0.2950	0.0744
	Sin/AG	0.0068	0.0068	0.4343	0.5390	0.1806	0.0214	0.2738	0.0764
	SinC/AG	0.0068	0.0068	0.4347	0.5393	0.1808	0.0214	0.4081	0.0600
	FSDT/AG	0.0068	0.0068	0.4337	0.5384	0.1804	0.0213	0.1416	0.0586

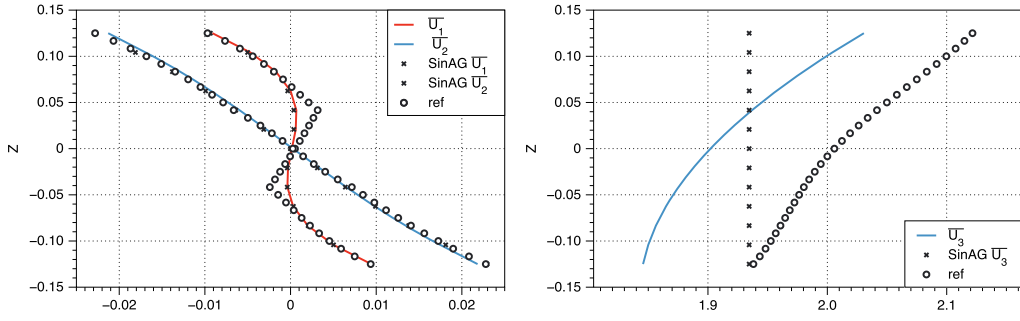


Figure 13.  $(0^\circ, 90^\circ, 0^\circ)$  square plate under mechanical load; distribution of  $\bar{U}_i$  for  $S = 4$ .

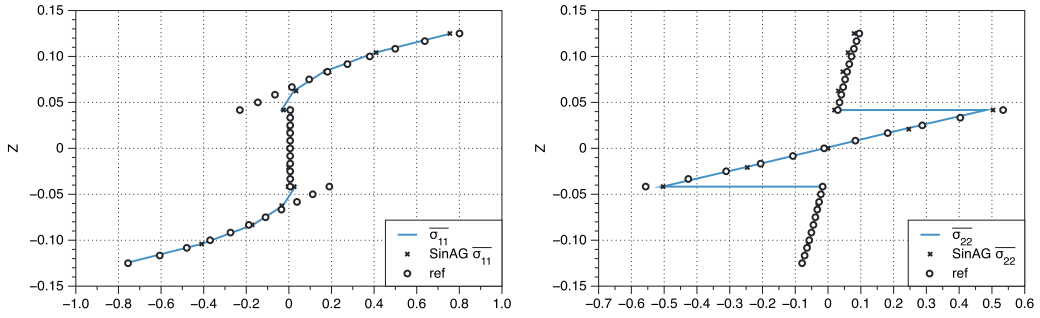


Figure 14.  $(0^\circ, 90^\circ, 0^\circ)$  square plate under mechanical load; distribution of  $\bar{\sigma}_{\alpha\alpha}$  for  $S = 4$ .

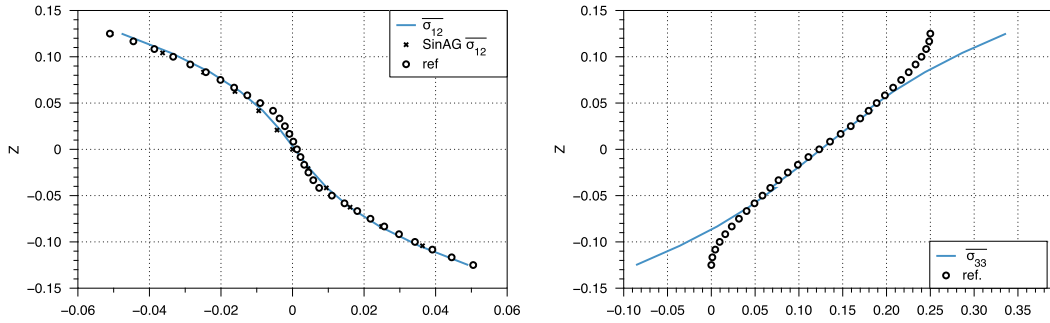


Figure 15.  $(0^\circ, 90^\circ, 0^\circ)$  square plate under mechanical load; distribution of  $\bar{\sigma}_{12}$  and  $\bar{\sigma}_{33}$  for  $S = 4$ .

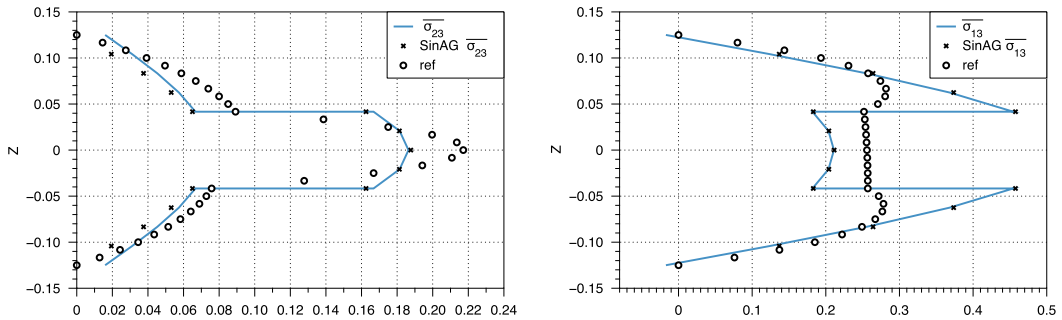


Figure 16.  $(0^\circ, 90^\circ, 0^\circ)$  square plate under mechanical load; distribution of  $\bar{\sigma}_{\alpha 3}$  for  $S = 4$ .

4.4.2. *Thermo-mechanical analysis.* This last test deals with a thermal load applied on a simply supported square laminated plate. The description of this test is the same as in the previous section

but the mechanical pressure load is replaced by an imposed temperature profile defined as follows:

$$T(x_1, x_2, z) = T_0 \frac{2z}{e} \sin \frac{\pi x_1}{a} \sin \frac{\pi x_2}{a} \quad (19)$$

Furthermore, the thermal expansion coefficients are defined by  $\alpha_T = 1125 \alpha_L$ .

The non-dimensional values are obtained using the following relations:

$$\bar{U}_\alpha = U_\alpha \frac{1}{T_0 \alpha_L a} \text{ for } \begin{cases} U_1(0, a/2, e/2) \\ U_2(a/2, 0, e/2) \end{cases} \quad \bar{U}_3 = U_3(a/2, a/2, e/2) \frac{e}{T_0 \alpha_L a^2};$$

$$\bar{\sigma}_{ij} = \sigma_{ij} \frac{1}{T_0 \alpha_L E_T} \text{ for } \begin{cases} \sigma_{11}, \sigma_{22}(a/2, a/2, e/2) \\ \sigma_{12}(0, 0, e/2) \\ \sigma_{13}(0, a/2, e/6), \sigma_{23}(a/2, 0, e/6) \end{cases}$$

As previously pointed out, the 3D constitutive law is essential to capture the full coupling between thermal load and induced stresses in the normal direction. The results are presented in Table VIII for different length-to-thickness ratios  $S$ , and comparisons are given with other FE. The reference solutions are given in [40]. For the thin plate case, the results obtained by the present FE are of same order than other results, but for the semi-thick and thick cases, a clear improvement is found, especially for the transverse displacement.

The distributions through the thickness for  $S = 10$  and  $S = 100$  are presented in Figures 17 and 18 for displacements and in Figures 19–22 for stresses. Comparisons are given with respect to exact solutions and Sin/AG results. A good agreement is recovered between present results and the reference solutions excepted for the transverse shear stress in Figure 22, where continuity condition at layer interfaces is not fulfilled by our present approach. The main difference between

Table VIII.  $(0^\circ, 90^\circ, 0^\circ)$  square plate under thermal load.

S	Model	$\bar{U}_1$	$\bar{U}_2$	$\bar{U}_3$	$\bar{\sigma}_{11}$	$\bar{\sigma}_{22}$	$\bar{\sigma}_{12}$	$\bar{\sigma}_{13}$	$\bar{\sigma}_{23}$
4	Ref.	-18.11	-81.83	42.69	1183.0	-856.1	-157.00	84.81	-128.70
	Sin-z2/CL8	-14.63	-72.51	46.87	906.0	-885.6	-137.00	56.29	-113.70
	Sin/AG	-14.78	-61.61	25.92	907.0	-918.4	-124.90	56.38	-111.00
	FSDT/AG	-9.12	-70.78	22.62	468.0	-896.4	-130.10	35.19	-117.30
10	Ref.	-16.61	-31.95	17.39	1026.0	-1014.0	-76.29	60.54	-66.01
	Sin-z2/CL8	-15.89	-29.65	17.67	970.0	-1021.0	-71.59	37.11	-73.93
	SIN/AG	-15.59	-27.69	14.13	945.0	-1026.0	-71.98	35.80	-73.72
	FSDT/AG	-14.21	-29.58	13.23	837.0	-1022.0	-72.88	21.82	-72.76
100	Ref.	-16.00	-16.17	10.26	965.4	-1065.0	-50.53	7.07	-7.08
	Sin-z2/CL8	-15.99	-16.14	10.26	966.5	-1064.0	-50.52	4.23	-8.39
	SIN/AG	-15.88	-16.12	10.16	958.8	-1064.0	-52.34	4.01	-8.31
	FSDT/AG	-15.87	-16.14	10.16	957.5	-1064.0	-52.40	2.43	-8.08
	CLT/AG	-15.89	-15.99	10.12	958.9	-1064.0	-51.70	—	—

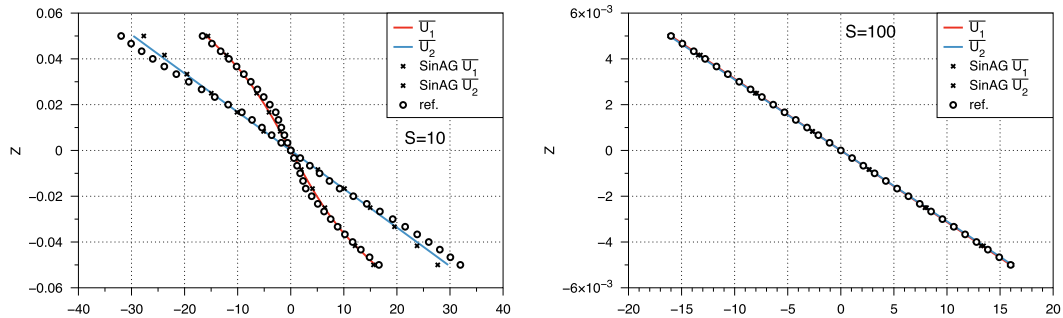


Figure 17.  $(0^\circ, 90^\circ, 0^\circ)$  square plate under thermal load; distribution of  $\bar{U}_\alpha$ .

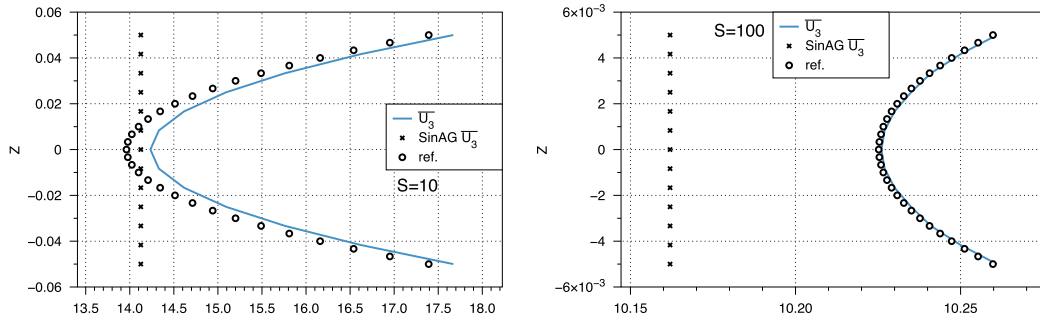


Figure 18.  $(0^\circ, 90^\circ, 0^\circ)$  square plate under thermal load; distribution of  $\bar{U}_3$ .

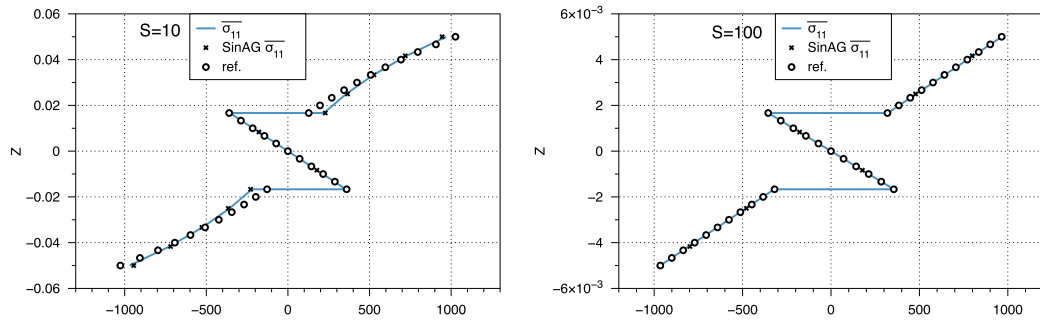


Figure 19.  $(0^\circ, 90^\circ, 0^\circ)$  square plate under thermal load; distribution of  $\bar{\sigma}_{11}$ .

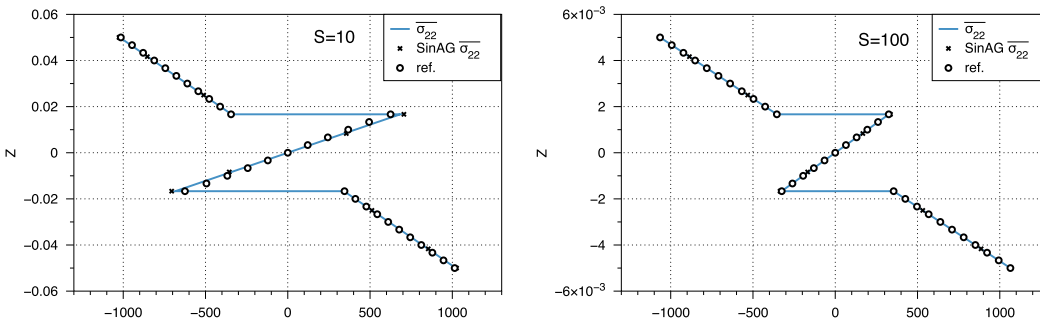


Figure 20.  $(0^\circ, 90^\circ, 0^\circ)$  square plate under thermal load; distribution of  $\bar{\sigma}_{22}$ .

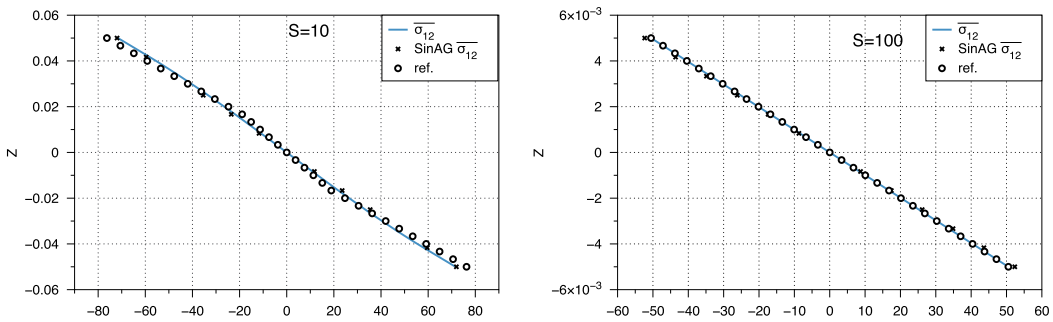


Figure 21.  $(0^\circ, 90^\circ, 0^\circ)$  square plate under thermal load; distribution of  $\bar{\sigma}_{12}$ .

Sin-z2/CL8 and Sin/AG concerns the transverse displacement, see Figure 18. Thanks to the choice of a non-constant variation of  $U_3$ , the present approach is in very good agreement with respect to the reference solution.

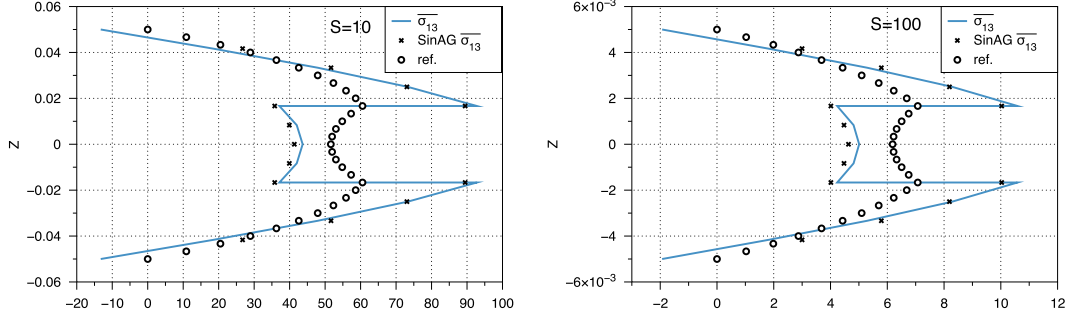


Figure 22.  $(0^\circ, 90^\circ, 0^\circ)$  square plate under thermal load; distribution of  $\bar{\sigma}_{13}$ .

## 5. CONCLUSION

In this paper, a new  $C^0$  FE has been presented on the basis of a refined sinus model, introducing only two supplementary unknown functions, and two more DOFs at each node, with respect to the classical FSDT model. The 3D constitutive law is used, using a specific refinement for the transverse displacement, avoiding the classical plate hypothesis, neglecting the transverse normal stress. Furthermore, a static condensation at the elementary level is used to eliminate the additional terms for the transverse displacement. Based on the sinus model, this approach does not need shear correction factor.

This FE is free of numerical illness such as transverse shear and Poisson lockings, oscillation and spurious mechanics. The methodology for the control of the transverse shear locking, previously introduced for the development of an FSDT FE, has been extended with success to this refined model.

The evaluation has been conducted for isotropic very thick-to-thin plates, and results are in good agreement with reference solutions. Distorted mesh for square and circular plates has been also evaluated to quantify the sensitivity to mesh distortion for different boundary conditions. Finally, a three-layered square plate submitted to mechanical and thermal loads has been also considered, leading to very promising results.

This new FE seems to be a very attractive tool for thick-to-thin plate as it shows a good compromise between cost and accuracy for displacements and stresses, under various boundary conditions and loads.

The present work could be a good starting point for the development of hierarchic approaches, as it has been performed for multilayered beam structures [23, 29], and for plates and shells in [20, 21, 27]. Therefore, future works are pointed towards a full evaluation of multilayered and sandwich plates and on the development of the associated shell FE.

## APPENDIX A: EXPRESSION OF THE THICKNESS MATRICES

The matrix  $[F_u(z)]$  (3, 9), associated with the displacement, is given by

$$[F_u(z)] = \begin{bmatrix} 1 & 0 & 0 & 0 & f(z) & f(z) - z & 0 & 0 & 0 \\ 0 & 1 & 0 & -f(z) & 0 & 0 & f(z) - z & 0 & 0 \\ 0 & 0 & 1 & 0 & 0 & 0 & 0 & z & z^2 \end{bmatrix} \quad (\text{A.1})$$

The matrix  $[F_\epsilon(z)]$  (6, 22), associated with the strain components, has its non-zero terms defined by

$$\begin{aligned} F_\epsilon(z)(1, 2) &= 1 & F_\epsilon(z)(1, 11) &= f(z) & F_\epsilon(z)(1, 14) &= f(z) - z \\ F_\epsilon(z)(2, 6) &= 1 & F_\epsilon(z)(2, 9) &= -f(z) & F_\epsilon(z)(2, 18) &= f(z) - z \\ F_\epsilon(z)(3, 19) &= 1 & F_\epsilon(z)(3, 20) &= 2z \end{aligned}$$

$$\begin{aligned}
F_\epsilon(z)(4, 7) &= -f'(z) & F_\epsilon(z)(4, 16) &= f'(z) & F_\epsilon(z)(4, 21) &= 1 \\
F_\epsilon(z)(5, 10) &= f'(z) & F_\epsilon(z)(5, 13) &= f'(z) & F_\epsilon(z)(5, 22) &= 1 \\
F_\epsilon(z)(6, 3) &= 1 & F_\epsilon(z)(6, 5) &= 1 & F_\epsilon(z)(6, 8) &= -f(z) \\
F_\epsilon(z)(6, 12) &= f(z) & F_\epsilon(z)(6, 15) &= f(z) - z & F_\epsilon(z)(6, 17) &= f(z) - z
\end{aligned}$$

## APPENDIX B: FINITE ELEMENT APPROXIMATIONS

### The eight node interpolation

The interpolation functions on the elementary domain are defined as follows:

$$\forall(\xi, \eta) \in [-1, 1]^2, \quad p(\xi, \eta) = \sum_{i=1}^8 Nq_i(\xi, \eta) p_i \text{ with}$$

$$\begin{aligned}
Nq_1(\xi, \eta) &= -\frac{1}{4}(1-\xi)(1-\eta)(1+\xi+\eta) & Nq_2(\xi, \eta) &= -\frac{1}{4}(1+\xi)(1-\eta)(1-\xi+\eta) \\
Nq_3(\xi, \eta) &= -\frac{1}{4}(1+\xi)(1+\eta)(1-\xi-\eta) & Nq_4(\xi, \eta) &= -\frac{1}{4}(1-\xi)(1+\eta)(1+\xi-\eta) \\
Nq_5(\xi, \eta) &= \frac{1}{2}(1-\xi^2)(1-\eta) & Nq_6(\xi, \eta) &= \frac{1}{2}(1+\xi)(1-\eta^2) \\
Nq_7(\xi, \eta) &= \frac{1}{2}(1-\xi^2)(1+\eta) & Nq_8(\xi, \eta) &= \frac{1}{2}(1-\xi)(1-\eta^2)
\end{aligned}$$

### The four node interpolation

$$\forall(\xi, \eta) \in [-1, 1]^2, \quad p(\xi, \eta) = \sum_{i=1}^4 Nl_i(\xi, \eta) p_i \text{ with}$$

$$\begin{aligned}
Nl_1(\xi, \eta) &= (1-c\xi)(1-c\eta)/4 & Nl_2(\xi, \eta) &= (1+c\xi)(1-c\eta)/4 \\
Nl_3(\xi, \eta) &= (1-c\xi)(1+c\eta)/4 & Nl_4(\xi, \eta) &= (1-c\xi)(1+c\eta)/4
\end{aligned} \quad \text{with } c = \sqrt{3}.$$

## REFERENCES

1. Mackerle J. Finite element linear and nonlinear, static and dynamic analysis of structural elements: a bibliography (1992–1995). *Engineering Computations* 1997; **14**(4):347–440.
2. Mackerle J. Finite- and boundary-element linear and nonlinear analysis of shells and shell-like structures : a bibliography (1999–2001). *Finite Elements in Analysis and Design* 2002; **38**:765–782.
3. Hughes T, Tezduyar T. Finite elements based upon Mindlin plate theory with particular reference to the four-node bilinear isoparametric element. *ASME - Journal of Applied Mechanics* 1981; **48**:587–596.
4. Bathe K, Dvorkin E. A four node plate bending element based on Mindlin–Reissner plate theory and a mixed interpolation. *International Journal for Numerical Methods in Engineering* 1985; **35**:503–519.
5. Somashekar B, Prathap G, Ramesh B. A field consistent four-node laminated anisotropic plate/shell element. *Computers & Structures* 1987; **25**:345–353.
6. Park K, Pramono E, Stanley G, Cabiness H. The ANS shell elements : earlier and recent improvements. In *Analytical and Computational Models of Shells*, Vol. 3, Noor AK, *et al.* (eds), 1989; 359–382.
7. Batoz J, Lardeur P. A discrete shear triangular nine DOF element for the analysis of thick to very thin plates. *International Journal for Numerical Methods in Engineering* 1989; **28**:533–560.
8. Simo JC, Rifai S, Fox DD. On stress resultant geometrically exact shell model. Part IV : variable thickness shells with through the thickness stretching. *Computer Methods in Applied Mechanics and Engineering* 1990; **81**:53–91.
9. Bletzinger KU, Bischoff M, Ramm E. A unified approach for shear-locking-free triangular and rectangular shell finite elements. *Computers & Structures* 2000; **75**:321–334.
10. Reddy JN. *Mechanics of laminated composite plates and shells. Theory and analysis*, Second ed. CRC Press, 2004.

11. Kapania K. A review on the analysis of laminated shells. *ASME - Journal of Pressure Vessel Technology* 1989; **111**(2):88–96.
12. Noor AK, Burton WS. Assessment of computational models for multilayered composite shells. *Applied Mechanics Reviews* 1989; **43**(4):67–97.
13. Reddy JN, Robbins DH. Theories and computational models for composite laminates. *Applied Mechanics Reviews* 1994; **47**(6):147–165.
14. Kant T, Swaminathan K. Estimation of transverse/interlaminar stresses in laminated composites—a selective review and survey of current developments. *Composite Structures* 2000; **49**:65–75.
15. Carrera E. Theories and finite elements for multilayered, anisotropic, composite plates and shells. *Archives of Computational Methods in Engineering* 2002; **9**(2):87–140.
16. Carrera E. Historical review of ZIGZAG theories for multilayered plates and shells. *Applied Mechanics Reviews* 2003; **56**:287–308.
17. Zhang Y, Yang C. Recent developments in finite elements analysis for laminated composite plates. *Composite Structures* 2009; **88**:147–157.
18. Yu W, Hodges DH, Volovoi VV. Asymptotically accurate 3D recovery from Reissner-like composite plate finite elements. *Computers & Structures* 2003; **81**:439–454.
19. Yu W, Hodges DH, Volovoi VV. Mathematical construction of a Reissner–Mindlin plate theory for composite laminates. *International Journal of Solids and Structures* 2005; **42**:6680–6699.
20. Polit O, Touratier M. A multilayered/sandwich triangular finite element applied to linear and nonlinear analysis. *Composite Structures* 2002; **58**(1):121–128.
21. Dau F, Polit O, Touratier M.  $C^1$  plate and shell finite elements for geometrically non linear analysis of multilayered structures. *Computers & Structures* 2006; **84**:1264–1274.
22. Vidal P, Polit O. A thermomechanical finite element for the analysis of rectangular sandwich beams. *Finite Elements in Analysis and Design* 2006; **42**:868–883.
23. Vidal P, Polit O. A family of sinus finite elements for the analysis of rectangular laminated beams. *Composite Structures* 2008; **84**:56–72.
24. Touratier M. An efficient standard plate theory. *International Journal of Engineering Science* 1991; **29**:901–916.
25. Touratier M. A refined theory of laminated shallow shells. *International Journal of Solids and Structures* 1992; **29**(11):1401–1415.
26. Ganapathi M, Patel B, Polit O, Touratier M. A  $c^1$  finite element including transverse shear and torsion warping for rectangular sandwich beams. *International Journal for Numerical Methods in Engineering* 1999; **45**(1):47–75.
27. Polit O, Touratier M. High order triangular sandwich plate finite element for linear and nonlinear analyses. *Computer Methods in Applied Mechanics and Engineering* 2000; **185**:305–324.
28. D’Ottavio M, Polit O. Sensitivity analysis of thickness assumptions for piezoelectric plate models. *Journal of Intelligent Material Systems and Structures* 2009; **20**:1815–1834.
29. Vidal P, Polit O. A refined sine-based finite element with transverse normal deformation for the analysis of laminated under thermomechanical loads. *Journal of Mechanics of Materials and Structures* 2009; **4**:1127–1155.
30. Polit O, Touratier M, Lory P. A new eight-node quadrilateral shear-bending plate finite element. *International Journal for Numerical Methods in Engineering* 1994; **37**:387–411.
31. Touratier M. A generalization of shear deformation theories for axisymmetric multilayered shells. *International Journal of Solids and Structures* 1992; **29**:1379–1399.
32. Büchter N, Ramm E, Roehl D. Three-dimensional extension of non-linear shell formulation based on the enhanced assumed strain concept. *International Journal for Numerical Methods in Engineering* 1994; **37**:2551–2568.
33. Parisch H. A continuum-based shell theory for non-linear applications. *International Journal for Numerical Methods in Engineering* 1995; **38**:1855–1883.
34. Tessler A. An improved plate theory of 1,2-order for thick composite laminates. *International Journal of Solids and Structures* 1993; **30**:981–1000.
35. Barut A, Madenci E, Heinrich J, Tessler A. Analysis of thick sandwich construction by a 3,2-order theory. *International Journal of Solids and Structures* 2001; **38**:6063–6077.
36. Carrera E, Brischetto S. Analysis of thickness locking in classical, refined and mixed plate theories. *Composite Structures* 2008; **82**(4):549–562.
37. Cheng S. Elasticity theory of plates and a refined theory. *ASME - Journal of Applied Mechanics* 1979; **46**:644–650.
38. Ganapathi M, Polit O, Touratier M. A  $c^0$  eight-node membrane-shear-bending element for geometrically non-linear (static and dynamic) analysis of laminates. *International Journal for Numerical Methods in Engineering* 1996; **39**:3453–3474.
39. Pagano NJ. Exact solutions for rectangular bidirectional composites and sandwich plates. *Journal of Composite Materials* 1970; **4**:20–34.
40. Bhaskar K, Varadan TK, Ali JSM. Thermoelastic solutions for orthotropic and anisotropic composite laminates. *Composites Part B: Engineering* 1996; **27B**:415–420.
41. Carrera E. Developments, ideas, and evaluations based upon Reissner’s mixed variational theorem in the modelling of multilayered plates and shells. *Applied Mechanics Reviews* 2001; **54**:301–329.
42. Carrera E. Theories and finite elements for multilayered plates and shells: a unified compact formulation with numerical assessment and benchmarking. *Archives of Computational Methods in Engineering* 2003; **10**(3):216–296.

43. Babuska I, Suri M. On locking and robustness in the finite element method. *SIAM Journal Numerical Analysis* 1992; **51**:221–258.
44. Bischoff M, Ramm E. On the physical significance of higher order kinematic and static variables in a three-dimensional shell formulation. *International Journal of Solids and Structures* 2000; **37**:6933–6960.
45. Klinkel S, Gruttmann F, Wagner W. A continuum based three-dimensional shell element for laminated structures. *Computers & Structures* 1999; **71**:43–62.
46. Demasi L.  $\infty^3$  plate theories for thick and thin plates: the generalized unified formulation. *Composite Structures* 2008; **84**:256–270.